



Highly thin film with aerosol-deposited perovskite quantum dot/metal oxide composite for perfect color conversion and luminance enhancement

Sunghoon Kim^{a,1}, Seokwoo Kang^{b,1}, Seungmin Baek^c, Jinouk Song^d, Na-Eun Mun^a, Hyukmin Kwon^b, Hyo-Geun Kwon^c, Yong-Jin Pu^e, Tae-Woo Lee^f, Seunghyup Yoo^d, Jong-Min Oh^{g,*}, Jongwook Park^{b,*}, Sang-Wook Kim^{c,*}

^a Department of Applied Chemistry Food Science and Technology, Dong-Eui University, Busan 47340, Republic of Korea

^b Integrated Engineering, Department of Chemical Engineering, Kyung Hee University, Gyeonggi 17104, Republic of Korea

^c Nanomaterials Laboratory, Department of Molecular Science and Technology, Ajou University, Suwon 16499, Republic of Korea

^d School of Electrical Engineering, Korea Advanced Institute of Science and Technology (KAIST), Daejeon 34141, Republic of Korea

^e RIKEN Center for Emergent Matter Science (CEMS), Wako, Saitama 351-0198, Japan

^f Department of Materials Science and Engineering, Seoul National University, Seoul, Republic of Korea

^g Department of Electronic Materials Engineering, Kwangjuon University, Seoul 01897, Republic of Korea

ARTICLE INFO

Keywords:

Perovskite quantum dots
Aerosol deposition
Color conversion
Scattering effect
OLED backlight

ABSTRACT

Erstwhile, displays using down-converting color changing medium utilized color filters as an essential part of clarifying the trade-off between true colors and transmittance. In this study, we report the development of a novel, smart process for producing thin luminescent films that completely convert colors and enhance light intensity. Highly dense films are prepared by the co-deposition of perovskite quantum dots and metal oxide particles as color conversion layers and scattering agents, respectively. These layers can be directly deposited on blue organic light-emitting diodes using ultrasonic-assisted aerosol deposition (UAD). This method can allow displays using a down-conversion system to streamline the process due to absence of color filters. Using this method, films can be a minimum of 3 μm thick for complete conversion of blue light, a quarter that of inkjet-printed films. We demonstrate 7,353 cd m^{-2} in green and 411 cd m^{-2} in red converted emissions with no blue light leakage. Furthermore, the developed technique was shown to be compatible with versatile patterning processes. For example, UAD may be combined with a fine-metal shadow mask to produce a pattern of 30- μm -diameter dots. Even without using a mask, the method still produces a pattern of 13 μm wide lines. This system provides a new approach that may serve as an alternative to inkjet printing.

1. Introduction

Display technologies have rapidly evolved and improved in a wide variety of parameters, such as high resolution, larger screen sizes, color saturation, wide viewing angles, and contrast ratio in flat-panel displays. This evolution has been driven by the breakthrough technological advances of liquid crystal displays (LCDs) and organic light-emitting diodes (OLEDs), which have been competing and dominating the flat-panel industry for the last decade or so [1,2]. Alternatively, micro-scale light emitting diodes (micro-LEDs) based on individual red-green-blue (RGB) chips, [3–5] and quantum dot light-emitting diodes (QLEDs) [6–9] technologies are outfitting emerging next-

generation displays, where each pixel provides its own illumination with outstanding color purity. However, realizing these advanced technologies in ultra-large panels will require a great technological leap forward, owing to the accompanying challenges of these technologies, such as device stability and process capability to pick and place fine pixel arrays. Meanwhile, quantum dot (QD)-enhanced LCDs deliver a wide range of real-to-life colors, owing to their narrower bandwidth than OLEDs [10–13]. Nevertheless, OLED displays have overcome the low stability by using organic materials, showing a much better contrast ratio, wider viewing angle, and faster response time than LCDs. Liquid crystals do not completely block out backlighting, therefore LCDs have fundamentally lower black levels than OLEDs with self-emission

* Corresponding authors.

E-mail addresses: jmOH@kw.ac.kr (J.-M. Oh), jongpark@khu.ac.kr (J. Park), swkim@ajou.ac.kr (S.-W. Kim).

¹ These authors contributed equally to this work.

[14–15]. However, despite remarkable advances in the two types of displays, termed “transmissive” and “emissive” technologies, some issues still need to be resolved. Regrettably, from the viewpoint of manufacturing large-area displays at present, the common drawback of both technologies is their reliance on color filters (CFs). In particular, RGB subpixels in large-size OLED TVs are currently produced with white OLEDs combined with CFs, not utilizing the full benefits of self-emissive displays [16–18]. Recently, novel display technologies have emerged, combining QDs and OLEDs as color conversion layers (CCLs) and a backlight, respectively. The QD – OLED hybrid system provides an excellent compromise between the crisp colors of QDs and the black levels of OLEDs. Some trials have reported patterning colloidal QDs using inkjet printing on blue OLED (BOLED) substrates to serve as excitation and blue light sources [19–21]. QD inkjet printing has been recognized as a state-of-the-art process technology that guarantees low material consumption and predesigned, mask-free fine patterns on demand. This process generally requires stringent conditions: fine nozzle head control to eject accurate volumes and to prevent nozzle clogging, specialized ink design to obtain a coffee-ring-free profile, and bank organization to determine pixel thickness, including compatibility with QD inks [22–25]. Inks containing scattering particles are ejected to enhance the optical properties of a panel, however the accuracy of ejecting the droplets into a specified position is severely reduced by nozzle clogging, and the scattering particles can sink to the bottom of the ink-filled pocket [26,27]. Furthermore, even if all of the above conditions are satisfied and QD inks for color conversion are applied, CFs are still required due to the limitations of the thickness and density of QDs derived from the inkjet process. When a CCL is inkjet-printed on top of a BOLED, blue-light emission from the BOLED is absorbed by the CCL and down-converted to green or red, depending on the size of QDs; however, a significant portion of the blue light can often leak owing to the limited absorption of the light-conversion layers. Previous studies indicate that CCLs thicker than approximately 12 μm are needed to avoid such leakage when using the inkjet printing method [19–21]. However, it is highly difficult to fabricate banks and CCLs thicker than 12 μm , due to the limited availability of any bank material guaranteed to be thicker than 12 μm and problems in drying such a thick CCL. Considering all the down-conversion systems reported so far in flat panel displays, including inkjet, CFs have been essential even in the presence of narrow bandwidth phosphors. In the current study, we overcome these issues by utilizing ultrasonic-assisted aerosol deposition (UAD) to manufacture thin CCLs with increased density, in order to prevent leakage of blue light. Lead halide perovskite nanocrystals demonstrate excellent color purity and high luminous efficiency levels, and can thus be used as light-emitting materials for CCLs [28–32]. The UAD technique enables very dense film formation by using perovskite quantum dot (PeQD) aerosols that reach the speed of sound. In addition, it has the advantage of not requiring complicated equipment, and the throughput time is relatively fast compared to other deposition equipment such as an evaporator and a sputtering system [33–36]. Based on this knowledge, we propose a smart design that employs UAD with PeQDs to create CF-free CCLs. Additionally, we demonstrate that metal oxide particles embedded in the CCLs not only helped prevent the leakage of blue-light emission, but also increased the light intensity due to the scattering effect, even in thinner CCLs. Furthermore, a patterned PeQD array was prepared with and without a mask in an additive fashion using the UAD method. In this study, PeQDs and metal oxide particles were co-deposited on the BOLED substrate using the UAD method to prevent leakage of blue light and maximize light conversion with high luminescence, further aiming to advance blue backlight displays applicable to mini-, micro-, and GaN nanorod LEDs.

2. Materials and methods

2.1. Chemicals and reagents

All reagents were used as received without further purification. PbO (99.9%), trioctylphosphine oxide (TOPO, 90%), CsCO_3 (99%), oleic acid (OA, 90%), oleylamine (OLA, 70%), ZnI_2 (98%), n-hexane (95%), methyl acetate (MeOAc, 99.5%), and 1-octadecene (ODE, 90%) were purchased from Sigma Aldrich. ZnBr_2 (98%) was purchased from TCI. ZnCl_2 (98%) was purchased from Samchun Chemical Co. All reagents used to prepare 2,12-di-*tert*-butyl-5,9-bis(4-(*tert*-butyl)phenyl)-7-methyl-5,9-dihydro-5,9-diaza-13b-boranaphtho[3,2,1-de]anthracene (BBK-204) and 2-(10-phenylanthracen-9-yl)naphtho[2,3-b]benzofuran (BBK-523) were purchased from Sigma-Aldrich and Alfa Aesar. All layers used in the BOLED device, including N,N-di(1-naphthyl)-N,N-diphenyl-(1,1-biphenyl)-4,4-diamine (NPB), tris(4-carbazoyl-9-ylphenyl)amine (TCTA), 1,3-bis(N-carbazoyl)benzene (mCP), and 1,3,5-tris(3-pyridyl-3-phenyl)benzene (TmPyPB) were purchased from Lumtec Corp. Spherical $\alpha\text{-Al}_2\text{O}_3$ (avg. diameter = 800 nm, 99.9%), and SiO_2 (avg. diameter = 800 nm, 99.9%) powders were purchased from US Research Nanomaterials, Inc.

2.2. Experimental details

2.2.1. Synthesis of TOPO-Zn PeQDs

Cs_2CO_3 (1.2 mmol) was dissolved in 12 mL of ODE with OA (6 mmol). The stock solution was degassed at 120 °C for 1 h. In another pot, PbO (1.0 mmol), ZnX_2 (X = Cl, Br, I, 10 mmol) TOPO (5 mmol), OA (22.5 mmol), and OLA (22.5 mmol) were degassed with ODE (25 mL) solvent at 120 °C for 1 h. After purging with N_2 , Cs-oleate (2 mL) was injected into the Pb-oleate pots at 230 °C. After cooling to 200 °C, the reaction pot was cooled to room temperature using an ice bath. The crude solution was centrifuged at 8000 rpm for 10 min. After sufficient drying, the collected precipitate was dispersed in hexane (15 mL) and centrifuged with MeOAc (15 mL) at 8000 rpm for 10 min. After dispersion in hexane, the product was filtered using a 0.2 μm polytetrafluoroethylene filter [37].

2.2.2. Preparation of the blue OLED device

ITO glasses (25 mm \times 25 mm) were sequentially ultrasonically washed in acetone, ethanol, deionized water, and isopropyl alcohol, and then dried in an oven at 80 °C. The substrates were further cleaned with a UV-ozone cleaner for 10 min before vacuum evaporation. In each of the EL devices, NPB was used as the hole injection layer (HIL), TCTA was used for the hole transporting layer (HTL), mCP was used for the HTL and electron blocking layer (EBL), BBK-523 and BBK-204 were used as the emitting layer (EML) in the host-dopant system, TmPyPB was used as the electron transporting layer (ETL) and hole blocking layer (HBL), lithium fluoride (LiF) was used as the electron injection layer (EIL), and ITO was used as the anode and Al as the cathode. All organic layers were deposited at 1.0×10^{-6} Torr, with a deposition rate of 1 \AA s^{-1} to create a 4 mm² emitting area.

2.2.3. Deposition of pristine PeQDs and PeQD/metal oxide composite layers

The UAD equipment consisted of an aerosol chamber, deposition chamber, and atomizer, as well as nozzles, carrier gases, and a vacuum system (Fig. 1a). A mechanical rotary pump was used to create near-vacuum conditions in the chambers, and UAD was used to deposit the PeQD films at 10^{-1} Torr at room temperature. CCL materials TOPO-Zn CsPbBr_3 (green) and TOPO – Zn CsPb(BrI)_3 (red) QDs, each at a concentration of 64 mg 100 mL⁻¹, were dispersed in n-hexane, and metal oxide powders ($\alpha\text{-Al}_2\text{O}_3$ or SiO_2) were percolated through a fine sieve net (ASTM mesh No. 170). These 4 materials were placed in 4 different aerosol chambers. The deposition of pristine PeQDs (green or red) was initiated by generating aerosolized droplets of the PeQD solution using

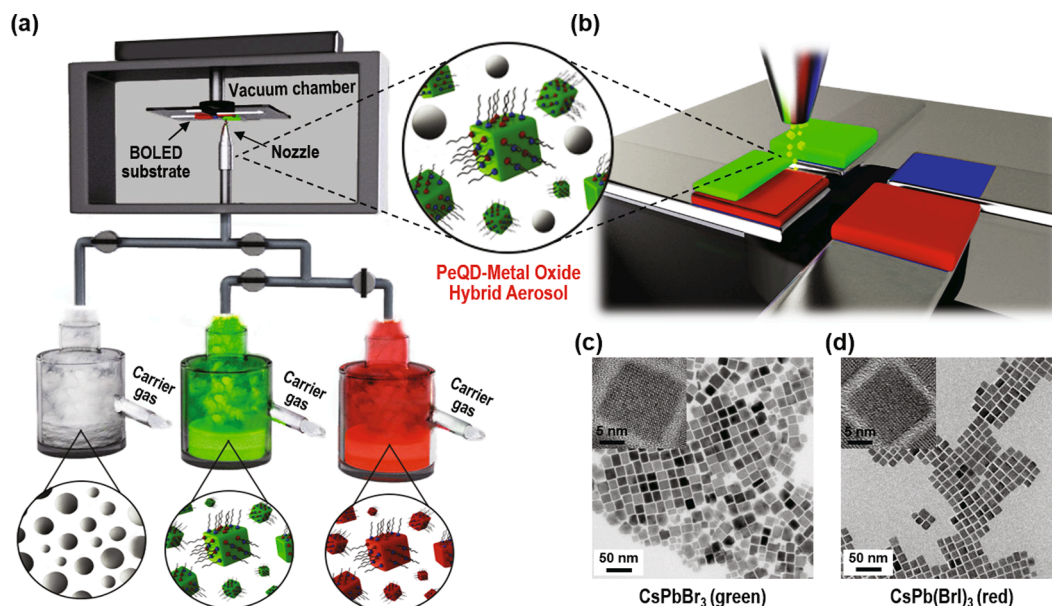


Fig. 1. PeQD CCLs on top of BOLED via UAD method. (a) Schematic illustration of co-deposition equipment used for green and red PeQD CCLs (N_2 carrier gas, under 10^{-1} torr). (b) Schematic illustration of the co-deposition of PeQDs and metal oxide on a BOLED device. High-resolution transmission electron microscopy images of (c) $CsPbBr_3$ QD and (d) $CsPb(Br)_3$ QD.

an ultrasonic atomizer (1.8 MHz) and N_2 carrier gas injected at a rate of 1 L min^{-1} . In mixtures of PeQDs and metal oxide, the two components were made to converge into the nozzle from each aerosol chamber for their subsequent co-deposition. To control the feeding amounts of PeQD and metal oxide, the mass flow controller was adjusted to control the flow rate of the N_2 carrier gas in the range $0.1\text{--}1.0 \text{ L min}^{-1}$. Then, the ultrasonically generated PeQD aerosol was quickly passed through the orifice nozzle (diameter = 1 mm) owing to the pressure difference between the aerosol and deposition chambers under the carrier gas flow. These aerosols were quickly ejected to the BOLED substrate located 5 mm away from the nozzle. The substrate holder attached to the BOLED substrate was automatically moved along the X–Y plane at a scanning speed of 5 mm s^{-1} . As a result, PeQD layers or PeQD/metal oxide composite layers were deposited in dense states on the BOLED substrate. The film thickness was varied by adjusting the PeQD concentration and the number of scans. To achieve the cutoff of blue light, CCLs were deposited in 3–4 scans with a PeQD concentration (green and red) of $64 \text{ mg } 100 \text{ mL}^{-1}$.

2.2.4. Optical simulation of the effect of scattering particles

A simple optical simulation was performed using a commercial ray-tracing-based Monte Carlo simulation (LightTools™) to observe the effect of scattering particles in the perovskite layer on the color conversion strength of the layer or luminance enhancement. In this optical simulation, a glass substrate attached to a single PeQD layer was considered.

At the opposite interface of the glass substrate from the perovskite layer, Lambertian light was set to enter the glass substrate. Here, it is assumed that the injected light can be absorbed by the PeQD layer and has only a single wavelength λ_{abs} . The absorbed light is intended to be fully converted into light with a single wavelength of λ_{emi} and emitted again into the PeQD layer. The reflectance of the interface where light enters is assumed to be 0.8, regardless of the wavelength and angle of the incident light. Then, each luminance value at wavelengths λ_{abs} and λ_{emi} was simulated for various values of $t_{\text{abs}}^{(\text{rel})}$ and scatterance. Here, the asymmetry parameter of the scattering in the PeQD layer was set to 0.9 throughout the layer [50].

2.2.5. Patterning processes with and without the use of masks

Dot-patterned films ($90 \text{ mm} \times 90 \text{ mm}$) of green or red PeQD/ SiO_2 composites on flexible substrates were prepared using the fine metal mask (FMM; diameter = $30 \mu\text{m}$) and UAD. The films were composed of dot patterns with a diameter and pixel gap of $30 \mu\text{m}$ when a mask was used. Mask-free lithographic patterning was successfully performed by modifying the internal geometry of the nozzle through which the sheath gas flowed. The key parameters for this geometry were the nozzle diameter ($100 \mu\text{m}$), the distance between the nozzle tip and the substrate ($<2 \text{ mm}$), and the focusing ratio (sheath gas flow rate/carrier gas flow rate). The line pattern width decreased as the focusing ratio increased, up to a focusing ratio of 5:1. Lines $100 \mu\text{m}$ and $13 \mu\text{m}$ in width were obtained at focusing ratios of 1:1 and 5:1, respectively.

3. Results and discussion

3.1. Description of PeQD-BOLED hybrid device

The PeQD-BOLED device was fabricated, as shown in Fig. 1a,b. The UAD method for perovskite film formation has three key advantages. First, the hybrid system using deposited PeQDs on a BOLED substrate helps the deposited layers convert light without CFs. Second, the reduction of the film thickness and the enhancement of the light intensity facilitated by the scattering effect of fine-sized metal oxide particles leads to an effective propagation length within the medium. Finally, a facile patterning process using a shadow mask, and direct-write patterns without using a mask were proposed for a full-color display with high resolution. Photo-stable $CsPbBr_3$ and $CsPb(Br)_3$ PeQDs passivated by a trioctylphosphine oxide (TOPO) – Zn complex were used as color conversion materials with green and red photoluminescence (PL) [37]. The QDs were well-arranged and uniform in shape (Fig. 1c,d). The optical properties of $CsPbBr_3$ and $CsPb(Br)_3$ are shown in Supplementary Fig. S1. The mixed aerosol flow was formed with PeQDs, fine metal oxide particles, and N_2 carrier gas under 10^{-1} Torr. Due to the carrier gas flow velocity of over 200 m s^{-1} [38], the mixed aerosol flow can embed the metal oxide particles in a dense PeQD matrix. BOLEDs of bottom emission were chosen with a highly efficient device [39,40] in order to apply blue light as a pump source. BOLEDs consisted of BBK-523 as a host material, which is based on a

dibenzofuran moiety, and BBK-204 as a dopant, using boron atoms based on multiple resonance effects. These materials were chosen because of the high external quantum efficiency (EQE) and narrow full width at half maximum (FWHM) previously reported by the patent (Supplementary Fig. S2) [41,42]. The photophysical properties of the synthesized organic materials are summarized in Supplementary Fig. S3 and Table S1. BBK-523 in the film state exhibited a maximum PL value of 443 nm. BBK-204 in the solution state had absorption and maximum PL values of 439 nm and 467 nm, respectively. Effective dopant materials use solution state data because dopant materials are low in concentration, e.g. 2% in the mixed film state. As a result, the PL spectrum of BBK-523 in the film state overlapped with the absorption spectrum of BBK-204 in the solution state, indicating that energy transfer could effectively occur. In particular, BBK-204 had a high photoluminescence quantum yield (PLQY) value of 83% and a narrow FWHM of 33 nm. The electroluminescence (EL) performance data of the device are summarized in Supplementary Fig. S4, S5 and Table S2. The peak wavelength and FWHM values of the EL emission were 458 nm and 25 nm, respectively, and the Commission Internationale de l'Éclairage (CIE) coordinate values were (0.136, 0.067) of deep blue. BOLED devices showed excellent EL performance as a backlight due to their narrow FWHM and excellent maximum quantum efficiency of 9.1%.

3.2. Preparation of PeQD deposition layers for complete color conversion

To reiterate, to optimize color conversion in fine-pixel RGB displays, blue light leakage through the CCLs should be prevented. However using the inkjet pixel-forming method, it is not possible for a PeQD or QD layer thinner than 12 μm to stop this leakage when the green or red conversion layer is placed on top of the BOLED [19,21]. In this study, UAD was used as a methodology, which can produce films dense enough to prevent the light leakage. In addition, commercial Al_2O_3 and SiO_2 particles were used as scattering agents. Metal oxide additives can induce a scattering effect inside films to effectively increase the propagation length within them, enabling both more effective prevention of blue light leakage and enhancement of the intensities of the emitted light. When CCL thickness is decreased, the bank thickness also decreases considerably. This decrease in bank thickness can reduce the light absorption of black-colored banks and, hence, provide higher device efficiency.

The PeQD film was produced using UAD from the ultrasonication of colloidal PeQD solution; the resulting dispersion was directly ejected toward the BOLED substrate with rapid N_2 carrier gas. In general, the inkjet printing method involves the use of a polymer binder component and several other additives, whereas UAD involves the use of relatively simple components like PeQDs and solvent [43–45]. As shown in Fig. 2a-c and e-g, 3 pairs of improved types of PeQD layers deposited on BOLED substrates were prepared: i) a dense film (thickness: 7.2 μm) of PeQDs, ii) a composite film (thickness: 3 μm) of PeQDs mixed with Al_2O_3 particles (feeding ratio: 30% to PeQD), and iii) a composite film (thickness: 3 μm) PeQDs mixed with SiO_2 particles (feeding ratio: 30% to PeQD). Spherical particles of metal oxide were evenly embedded, rather than sinking to the bottom of the PeQD layers, when using the co-deposition process. This embedding was confirmed using energy dispersive X-ray spectroscopy (EDS) (see Supplementary Fig. S6). We were able to tune the thickness of the deposited layers as desired, from approximately 1 to 10 s of micrometers, by adjusting the PeQD aerosol concentration and number of scans. A maximum film thickness of 34 μm was achieved without using any binders (see Supplementary Fig. S7).

When the UAD method was used, the minimum CCL thickness that yielded no blue-light leakage was 7.2 μm , much less than the minimum CCL thickness required to stop blue light leakage when using inkjet printing (Fig. 2a,e). This difference was attributed to UAD being able to produce denser films with more efficient energy conversion. In the PeQD/metal oxide composite layers for the scattering accelerated CCLs, the minimum CCL thickness still preventing some leakage of blue light was < 3 μm , (Fig. 2b-d and f-h). Blue-light leakage peaks were however

observed when using 3 μm thick pristine CsPbBr_3 (green) and $\text{CsPb}(\text{BrI})_3$ (red) QD CCL films without any metal oxide additive (Supplementary Fig. S8). The PL spectra and photographs from the 6 film samples indicate that blue light emission was perfectly blocked. The 6 films on top of the BOLEDs showed PL emissions of green and red light with peak wavelengths of 518 nm and 623 nm and peak FWHMs of 23 and 38 nm, respectively, i.e., there were no differences in the peak wavelength and FWHM between the PeQD/metal oxide composite films and pristine QD films. To the best of our knowledge, this work represents the first instance of eliminating the leakage of blue light by PeQD/metal oxide composite films through UAD. The methodology developed in this work is expected to be applicable to full-color displays that utilize fine RGB pixels.

The operating device consisted of 4 positions: i) pure BOLED, ii) red $\text{CsPb}(\text{BrI})_3$ CCL on a BOLED, iii) green CsPbBr_3 CCL on a BOLED, and iv) red/green CCLs on a BOLED. In the white emitting case (Fig. 1b), a red CCL, an optical clear film, and a green CCL were deposited stepwise onto the BOLED, whilst controlling the thickness of each layer. White light consists of three primary colors, at wavelengths of 462, 515, and 618 nm, respectively (Fig. 2j). These results were attributed to green and red colors solely originating from perfect down-conversion on top of the BOLED. Fig. 2k shows the color performance of the integrated device. The color coordinates of the locations for the prepared device were found to be (0.136, 0.067) for blue light, (0.157, 0.739) for green light, and (0.671, 0.327) for red light. It thus reached a wide color gamut: 115.0% of the National Television System Committee (NTSC) standard and 85.8% of the International Telecommunication Union (ITU) Recommendation BT 2020 (Rec. 2020) standard. The white-light CIE coordinates were (0.327, 0.326), which indicated the emission of pure white light.

3.3. Enhancement of down-conversion intensity

The BOLED showed a maximum luminance of 5,022 cd m^{-2} at 10 V. The down-converted maximum luminous intensities were 4,234 cd m^{-2} (pristine), 6,765 cd m^{-2} (Al_2O_3), and 7,353 cd m^{-2} (SiO_2) at 10 V for the 3 samples with the green CCL, and 257 cd m^{-2} (pristine), 367 cd m^{-2} (Al_2O_3), and 411 cd m^{-2} (SiO_2) at 9 V for the 3 samples with the red CCL. That is, for both the green and red CCLs, the device with the SiO_2 CCL whereby a SiO_2 aerosol flow rate of 0.3 L min^{-1} was applied, exhibited the highest luminance value at any given voltage. The maximum luminance of green and red CCL occurs at driving voltages of 10 V and 9 V, respectively. The reason why the red CCL showed maximum luminance at 9 V, not 10 V is that the photo stability of the red PeQD is relatively low. It means that the degradation occurs at high luminance of blue backlight. Moreover, when measuring the L-V curve, the degradation effect also should be considered by continuously irradiating light from 0 V to 10 V. Meanwhile, these measurements revealed that the Al_2O_3 device showed a higher luminance than the pristine CCL device, but less than the SiO_2 device (Fig. 3a,b). Table S3. Summarizes the data of brightness and its converted ratio according to the metal oxide additives. The luminance conversion ratio of green was higher than that of red emission, and the reason is that the stoke shift of red was larger from blue compared to green emission. As a result, the light conversion efficiency was relatively low. In addition, the light conversion efficiency was increased as the metal oxide was added than that of pristine. In particular, the brightness conversion ratio using SiO_2 was higher than that of Al_2O_3 . The PLQY of metal oxide embedded PeQD layers were also measured. The PLQY of pristine CsPbBr_3 , $\text{CsPbBr}_3/\text{Al}_2\text{O}_3$, and $\text{CsPbBr}_3/\text{SiO}_2$ were 15.8, 22.2, and 30.4%, respectively. In cases of $\text{CsPb}(\text{BrI})_3$, the values of 14.8, 17.8, and 20.2% were confirmed (Supplementary Fig. S9). Although the devices with metal oxide additives were each made with a thin CCL, i.e., only 3 μm thick, (for no leakage of blue light) they nevertheless yielded greater luminances than the pristine devices with a 7.2 μm CCL. As a result, when blue light was irradiated onto the PeQD/metal oxide composite layer, the light conversion efficiency was

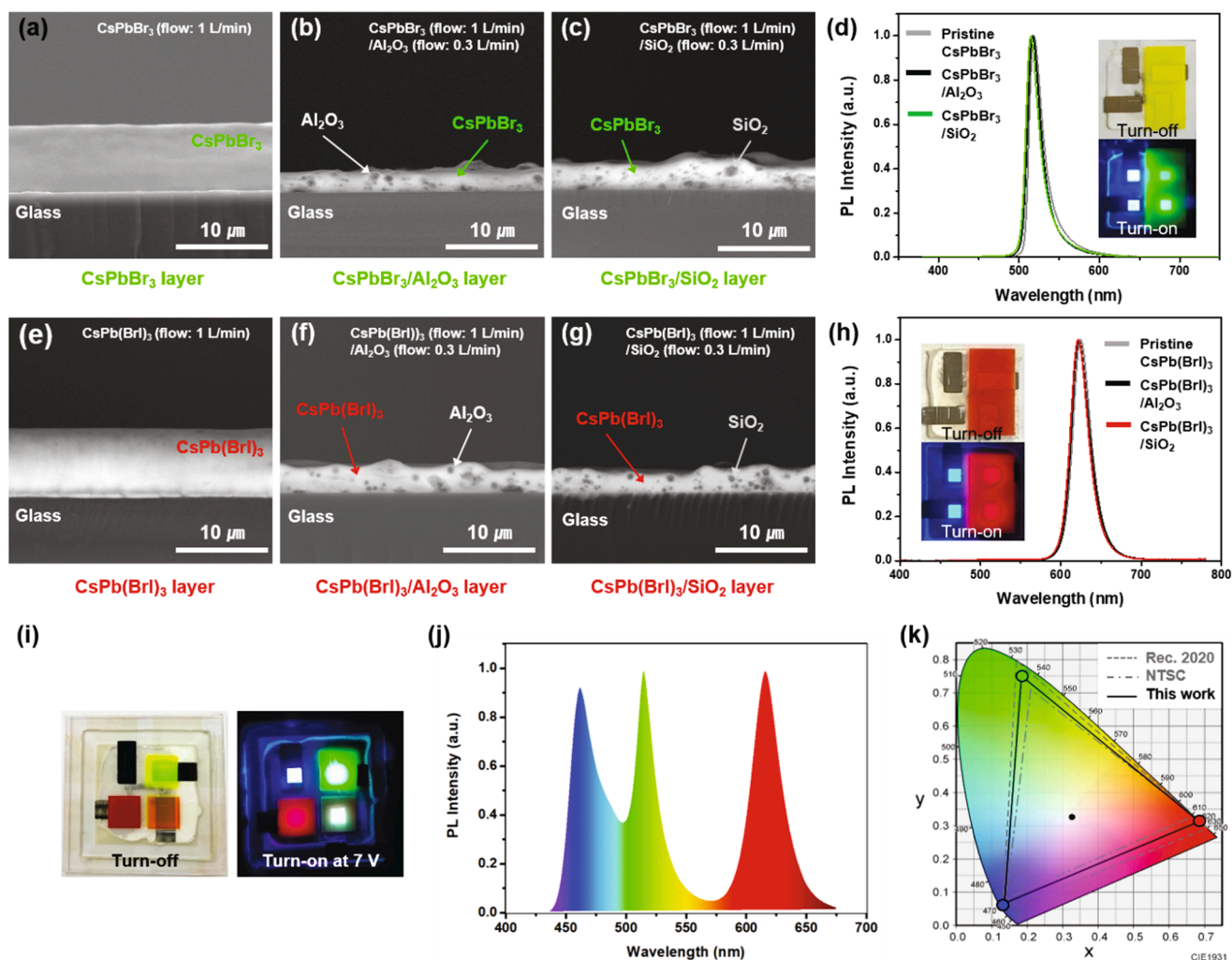


Fig. 2. Thicknesses of optimized color conversion layers without blue light leakage and their PL spectra originating from the BOLED light source. Cross-sectional scanning electron microscope (SEM) images of (a) CsPbBr₃ (thickness: 7.2 μm), (b) CsPbBr₃/Al₂O₃ (thickness: 3 μm), (c) CsPbBr₃/SiO₂ (thickness: 3 μm), (e) CsPb(BrI)₃ (thickness: 7.2 μm), (f) CsPb(BrI)₃/Al₂O₃ (thickness: 3 μm), and (g) CsPb(BrI)₃/SiO₂ (thickness: 3 μm). PL spectra of the optimized conversion layers containing (d) CsPbBr₃ and (h) CsPb(BrI)₃ exposed to blue-light BOLED emission (inset: photographs of integrated devices with PeQD layers embedded SiO₂). (i) Photographs of the PeQD – BOLED device showing RGB and white light emissions. (j) White-light emission spectra under the BOLED operation in the case of thin layer (<2 μm) depositions of CsPb(BrI)₃ and CsPbBr₃ PeQDs. (k) The color coordinates of BOLED blue light converted to green and red light, and the white-light emission under the device operation in the 1931 CIE chromaticity diagram along with NTSC and Rec. 2020 standard color references.

maximized. This result was due to the embedded metal oxide particles leading to the scattering effect, according to the theory described by Mie for dispersed particles, which is based on the difference in the refractive index (RI) of a host medium and particles [46,47]. Devices in the current work were developed to provoke the Mie scattering effect by incorporating spherical Al₂O₃ (RI = 1.77 at 520 nm) and SiO₂ (RI = 1.46 at 520 nm) particles [48,49]. Consequently, the luminance intensity values of the PeQD/metal oxide composite layers increased by 36.1% (green) and 29.9% (red) when Al₂O₃ particles were used, compared to the pristine PeQD layer, and increased by 42.4% (green) and 37.4% (red) higher when SiO₂ particles were used. Notably, the SiO₂-embedded composite layer exhibited an 8.1% higher luminance for the emission of green light than the Al₂O₃-embedded composite layer. This difference was attributed to the RI difference between SiO₂ (RI = 1.46 at 520 nm) and the PeQD matrix (1.72 at 520 nm) being greater than the RI difference between Al₂O₃ (RI = 1.77 at 520 nm) and the PeQD matrix. The relative viewing angle differences between PeQD and PeQD/metal oxide composite layers showed that slightly wider angles were observed for both green-light and red-light emissions of the composite over the pristine layers (insets of Fig. 3a,b). The devices with the SiO₂ additive showed intensities that, at all measured angles, were approaching the same as

those found for the devices with the Al₂O₃ additive.

Furthermore, by optimizing the SiO₂ aerosol feeding flow rate, we determined the appropriate amount of SiO₂ scattering particles to embed in the PeQD matrix to prevent the blue light leaking and to achieve increased light intensity (Fig. 3c,d). When a SiO₂ aerosol flow rate of 0.1 L min⁻¹ was applied, an additional peak corresponding to blue light was observed in the green-light emission spectrum, and a luminance of 5,564 cd m⁻² at 10 V was measured. Conversely, when aerosol flow rate of 0.5 L min⁻¹ were applied, not only did the absence of blue light peak, but luminance value of 6,486 cd m⁻² at 10 V, respectively, were measured. In other words, the greatest brightness in this series was observed at an aerosol flow rate of 0.3 L min⁻¹. At 0.5 L min⁻¹, the CCL had an opaque appearance to the naked eye. In addition, SEM images revealed that the aerosol flow rate was related to the amount of embedded SiO₂.

In order to evaluate the stability of the device, PL brightness was measured by the time (Figure S10). LT₅₀ of blue OLED device was 230 min. For the devices of pristine, Al₂O₃, and SiO₂, LT₅₀ of the converted green PL was 26.3, 26.9, and 28.1 min, respectively. For the converted Red, LT₅₀ was 13.5, 12.3, and 13.1 min, respectively. Comparing the LT₅₀ stability of the three samples for both green and red, we could

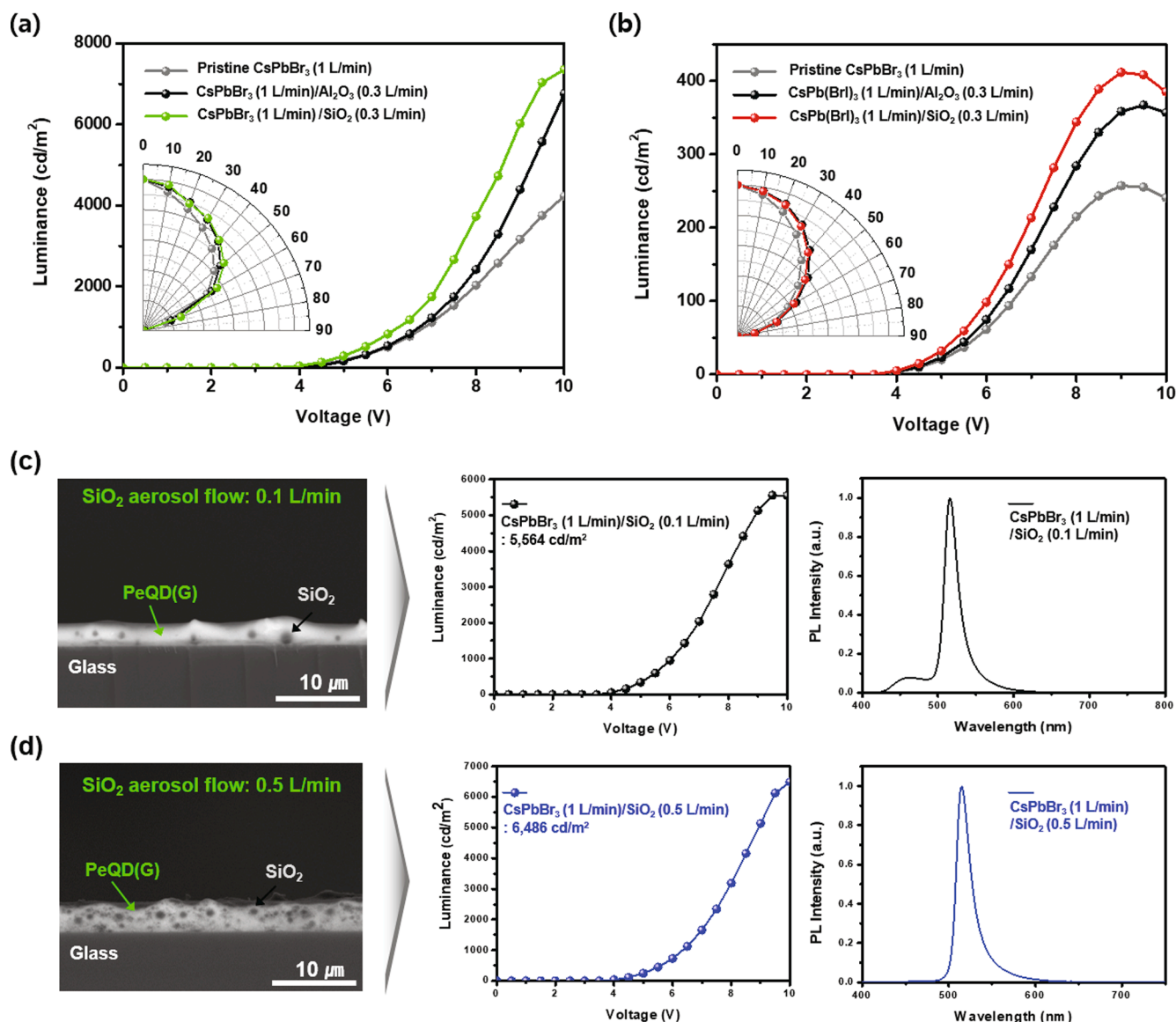


Fig. 3. Performance of luminance resulting from adding metal oxide particles embedded in PeQD layers. Luminance versus voltage curves of (a) CsPbBr₃ and (b) CsPb(Br)₃ layers each with or without metal oxide particles (Al₂O₃ or SiO₂) (insets: relative viewing angle differences of PeQD and PeQD/metal oxide composite layers). Cross-sectional SEM images, luminance, and PL spectra according to the amount of SiO₂ embedded in the PeQDs host matrix, respectively. (c) SiO₂ aerosol flow: 0.1 L min⁻¹ and (d) SiO₂ aerosol flow: 0.5 L min⁻¹.

observe that there is no decrease according to the metal oxide addition. As a result, we could conclude that the embedded metal oxide for the scattering effect does not affect the stability of the perovskite CCL layer. In the case of red perovskite CCL, the PL life-time is relatively shorter than that of green emission because the photo stability of the red perovskite emitter is low.

3.4. Optical simulations for scattering effects

To elucidate why the metal oxide additives can greatly influence the color conversion efficiency of the proposed PeQD layer and the luminance of the devices adopting them as CCLs, optical simulation was performed by tracing the rays propagating inside the PeQD media containing the metal oxide particles (see the Materials and methods for details). In the simulation, the light incident from the BOLED was assumed to have a single wavelength of λ_{abs} (blue light in a real device) for simplicity. Likewise, light converted from the absorbed light was assumed to have a single wavelength of λ_{emi} (green or red light in a real device).

Fig. 4a,b present the luminance at λ_{abs} and λ_{emi} ($=L_{\text{abs}}$ and L_{emi}), respectively, simulated as a function of the scatterance (S) and the normalized thickness of the PeQD layer ($=t_{\text{abs}}^{(\text{rel})}$). The PeQD layer thickness is normalized to the penetration depth ($=1/\alpha_{\text{abs}}$) at λ_{abs} to indicate how thick the PeQD layer is in terms of absorption of blue light delivered from OLEDs. The PeQD far thicker than $1/\alpha_{\text{abs}}$ (*i.e.* $t_{\text{abs}}^{(\text{rel})} \gg 1$) can be considered thick enough for sufficient absorption, for example. Scatterance (S) in scattering is analogous to absorbance in absorption phenomena. Practically speaking, S of n corresponds to the case where the thickness of a scattering layer is n times the mean free path (l_{free}) of scattering events. That is, S may be regarded as the thickness of a scattering layer normalized to l_{free} . $S \gg 1$ means that a layer is thick enough for a significant number of scattering events to occur [50]. Note that L_{abs} and L_{emi} correspond to the leaked and converted emission, respectively. As shown in the Fig. 4a, L_{abs} is reduced by a significant degree for a given $t_{\text{abs}}^{(\text{rel})}$ when S is increased. Likewise, the $t_{\text{abs}}^{(\text{rel})}$ required for a given L_{abs} is smaller when S is large, which is consistent with the experimental result that the PeQD/metal oxide composite layers are more efficient at

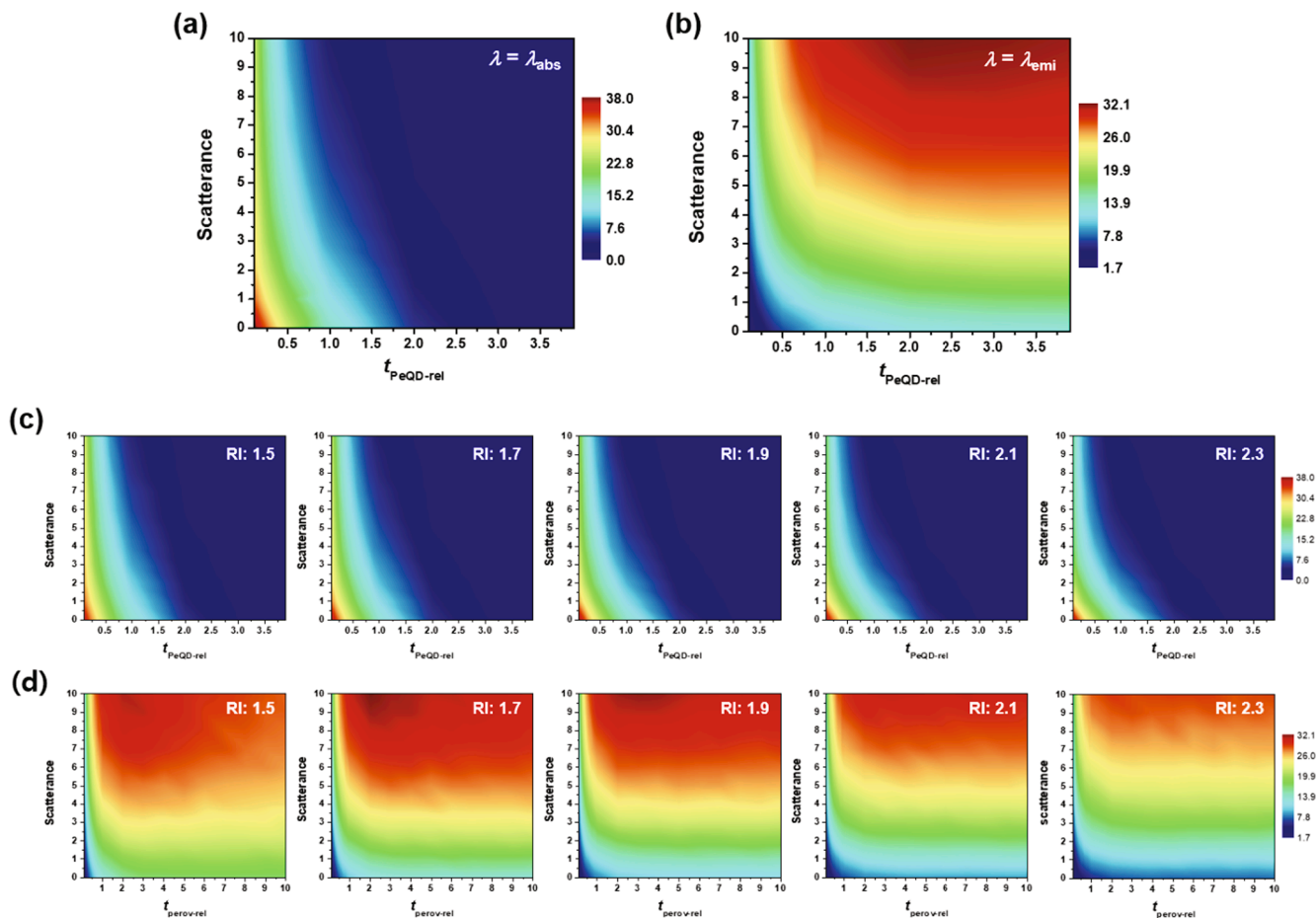


Fig. 4. Simulated relative luminance: scatterance as a function of $t_{\text{abs}}^{(\text{rel})}$ at (a) the absorption wavelength (λ_{abs}) and (b) the emission wavelength (λ_{emi}). Simulated relative luminance as a function of $t_{\text{abs}}^{(\text{rel})}$ and scatterance according to the refractive index (RI) of the PeQD layer at (c) absorption wavelength (λ_{abs}) and (d) emission wavelength (λ_{emi}).

preventing blue light leakage than pristine PeQD layers, even when thinner.

It is also noteworthy from Fig. 4a that L_{abs} approaches zero, *i.e.*, blue leakage is almost completely suppressed, provided that $t_{\text{abs}}^{(\text{rel})}$ is larger than *ca.* 2 regardless of S . Conversely, L_{emi} increases with S for all thickness ranges considered (Fig. 4b). This result indicates that a large portion of converted light is still confined in the PeQD films, and therefore, adding scattering particles is beneficial in further enhancing L_{emi} by outcoupling some of the confined light. Note that the increasing trend of L_{emi} vs. S mentioned above is similar to what was observed in a system presented in Ref. 49 which consists of an OLED in which a scattering film (nanoparticles embedded in a clear resin) with the asymmetry parameter close to unity is attached to the back of its substrate. This similarity is understandable because the present system is also expected to have a relatively high asymmetry parameter close to 0.9 from the relatively low index difference between the host and the scatterers and the relatively large size of the scattering particles.

However, one should be reminded that the present simulation focuses on illustrating the beneficial effect of scattering particles and thus there are several assumptions made for the sake of simplicity. For example, the present simulation assumes PLQY of the down-conversion process is unity and thus the medium is essentially lossless. In actual systems, however, PLQY of the down-conversion is often limited and thus a certain portion of the photons may simply be absorbed and converted into heat (loss mechanism.). For this reason, the effective propagation length within the host medium increased too much with a relatively high S could also lead to increased photon loss; hence, there

can be an optimal concentration of particles (proportional to S) where L_{emi} becomes the highest, as was the case for the experimental results shown in Fig. 3.

3.5. PeQD patterns produced using versatile UAD processes

Fine pixels, such as dot or strip patterns, are needed to fabricate a full-color display with high density resolution. The PeQD patterning achieved using UAD was examined with the aim to optimize the incorporation into commercially forthcoming QD – OLED displays. Two schematic illustrations of deposition, using a shadow mask and mask-free direct patterning, respectively, were considered (Fig. 5a,b). Unlike the photolithography process, shadow masking coupled with UAD was designed as a one-step process for fabricating high-quality patterned PeQD arrays. This simplified process eliminates several steps associated with developing, etching, stripping, washing, and cleaning. The dot patterns resulting from using the FMM were deposited by rapidly ejecting mixed aerosols of SiO_2 particles and PeQDs on flexible poly (ethylene terephthalate) substrates. Fine dotted pixels for green and red emissions were designed with a dot diameter of 30 μm and cell gap of 30 μm , according to inspection of the confocal images (Fig. 5c-f). These dot-patterned green and red films corresponded to a resolution of 424 dots per inch and were obtained on large substrates (90 \times 90 mm) at a school laboratory scale without a clean room (see Supplementary Fig. S12). This process can be applied to display panels employing FMMs in industry.

As an alternative approach, direct writing of the PeQD aerosol was

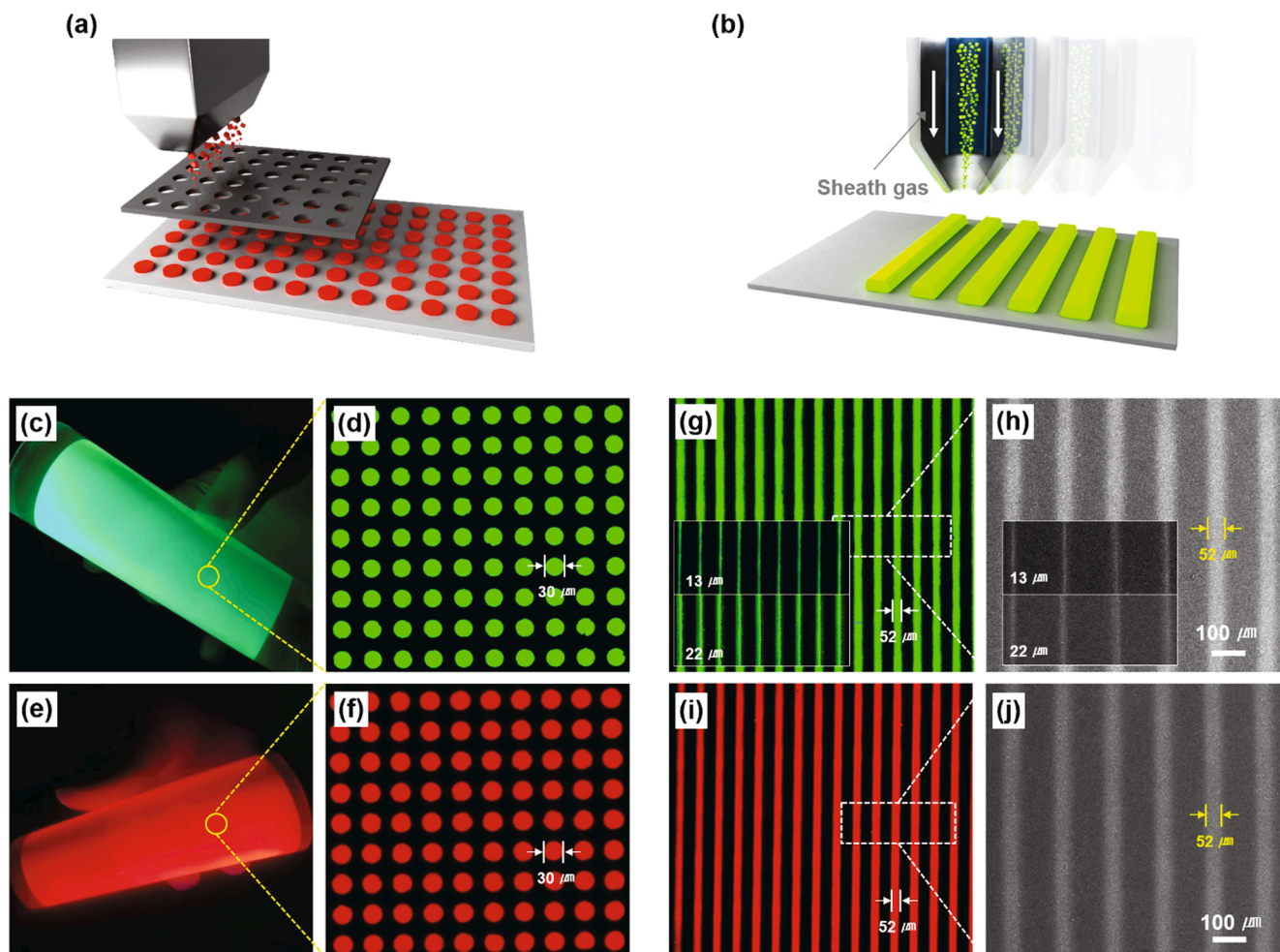


Fig. 5. Implementation of various patterns of PeQDs using the UAD process. Schematic diagrams of the patterns made using (a) the FMM and (b) mask-free methods. Photographs of (c) green and (e) red PeQDs deposited using the UAD method with a mask on a flexible PET film (90×90 mm). Magnified confocal fluorescence microscopy images of patterned deposited (d) green and (f) red films. (g-j) Confocal fluorescence microscopy and SEM images of strip-patterned films using direct writing methods (insets: thinner strip-line images of patterns with line widths of 13 and 22 μm).

achieved by adjusting the nozzle geometry to reflect the aerosol jet printing method [51,52]. For mask-free pattern preparation, UAD with a sheath gas-induced nozzle, without a shadow mask or laser trimming, produced a strip pattern (Fig. 5b). The geometry of the nozzle through the coaxial sheath gas flowed was able to decrease the polydispersity of the central PeQD aerosol. Consequently, the sheath gas ejected from the outer portion of the PeQD flow tube helped produce a pattern of narrow lines. Additionally, the widths of the lines in the patterns were controlled by adjusting the ratio of the sheath gas flow rate to the carrier gas flow rate. The ratio of the sheath gas flow rate to the carrier gas flow rate of the central PeQD emitter was 3:1 during this process. Green and red patterns with a line width of 52 μm and line spacing of 100 μm were successfully achieved according to the confocal fluorescence microscope images and their corresponding SEM images (Fig. 5g-j). In order to make the emission lines thinner, the above ratio was changed from 3:1 to 4:1 and then to 5:1. This change narrowed the deposition flow and the focus of the film deposition, which produced a thinner strip line: 22 μm with a 4:1 ratio, and 13 μm with a 5:1 ratio (insets of Fig. 5g,h). The larger volume of sheath gas caused the PeQD aerosol to be confined to the center of the flow. It was also found that although the line patterns became thinner as the ratio of the sheath gas flow increased, the uniformity of the lines decreases at a ratio greater than 6:1 (Supplementary Fig. S13). We would expect that the strip width can be narrowed even further to < 10 μm , if industrial equipment is utilized [53,54].

4. Conclusion

We deposited PeQD layers on top of BOLED backlights using UAD, where the use of a 7.2- μm -thick, almost half that of the inkjet-printed method, PeQD layer resulted in essentially perfect blocking of blue light leakage. When Al_2O_3 and SiO_2 particles were embedded in the PeQD matrices, light leakage was effectively prevented even in layer thicknesses as small as 3 μm . With these metal oxide additives, luminance intensity from the BOLED to the CCL effectively increased; e.g., increases of 42.4% (green) and 37.4% (red) with SiO_2 particles compared to the CCL without metal oxide particles as scattering agents. Two methods were used for PeQD array patterns: direct writing and shadow masking methods. The direct writing method provided the narrowest line patterns (13 μm), which is important for achieving high display resolution and simplifying the patterning process. These results are expected to be applied to real PeQD-BOLED displays in the near future.

Declaration of Competing Interest

The authors declare that they have no known competing financial interests or personal relationships that could have appeared to influence the work reported in this paper.

Acknowledgment

This study was supported by the National Research Foundation of Korea (NRF) under the Ministry of Science, ICT & Future Planning (Basic Science Research Program (No.2021R1A5A6002853, 2020R1A2C1004943, 2021M3H4A3A01062960, 2020M3A7B4002030, 2020R1A6A1A03048004, 2020R1G1A1102045, 2020R1F1A1073491) and Nano-Material Technology Development Program (No. 2017M3A7B4041696), Republic of Korea. Additionally, this work was supported by a Research Grant from Kwangwoon University in 2021, Korea Institute for Advancement of Technology (KIAT) grant funded by the Korea Government (MOTIE) (P0012451, The Competency Development Program for Industry Specialist) and National Research Facilities & Equipment Center of Korea Basic Science Institute (No. 2019R1A6C1010052).

Appendix A. Supplementary data

Blue OLED fabrication, UV-Vis absorption and PL spectra, I–V–L curve, SEM, EDS mapping, RI index, CCL photographs, simulation data (PDF). Aerosol deposited CCLs on BOLED operation (MP4). Supplementary data to this article can be found online at <https://doi.org/10.1016/j.cej.2022.135991>.

References

- H.W. Chen, J.H. Lee, B.Y. Lin, S. Chen, S.T. Wu, Liquid crystal display and organic light-emitting diode display: present status and future perspectives, *Light Sci. Appl.* 7 (2018) 17168. <https://doi.org/10.1038/lsa.2017.168>.
- E.L. Hsiang, Z. Yang, Q. Yang, Y.F. Lan, S.T. Wu, Prospects and challenges of mini-LED, OLED, and micro-LED displays, *J. Soc. Inf. Disp.* 29 (2021) 446–465, <https://doi.org/10.1002/jsid.1058>.
- S.-I. Park, Y. Xiong, R.-H. Kim, P. Elvikis, M. Meitl, D.-H. Kim, J. Wu, J. Yoon, C.-J. Yu, Z. Liu, Y. Huang, K.-C. Hwang, P. Ferreira, X. Li, K. Choquette, J.A. Rogers, Printed assemblies of inorganic light-emitting diodes for deformable and semitransparent displays, *Science* 325, *Science* 325 (5943) (2009) 977–981.
- J.Y. Lin, H.X. Jiang, Development of microLED, *Appl. Phys. Lett.* 116 (2020) 10052, <https://doi.org/10.1063/1.5145201>.
- Z. Liu, C.H. Lin, B.R. Hyun, C.W. Sher, Z. Lv, B. Luo, F. Jiang, T. Wu, C.H. Ho, H. C. Kuo, J.H. He, Micro-light-emitting diodes with quantum dots in display technology, *Light Sci. Appl.* 9 (2020) 83, <https://doi.org/10.1038/s41377-020-0268-1>.
- H. Zhang, S. Chen, X.W. Sun, Efficient red/green/blue tandem quantum-dot light-emitting diodes with external quantum efficiency exceeding 21%, *ACS Nano* 12 (2018) 697–704, <https://doi.org/10.1021/acsnano.7b07867>.
- M.K. Choi, J. Yang, T. Hyeon, D.H. Kim, Flexible quantum dot light-emitting diodes for next-generation displays, *Npj Flex. Electron.* 2 (2018) 1–14, <https://doi.org/10.1038/s41528-018-0023-3>.
- M. Liu, N. Yazdani, M. Yarema, M. Jansen, V. Wood, E.H. Sargent, Colloidal quantum dot electronics, *Nat. Electron.* 4 (2021) 548–558, <https://doi.org/10.1038/s41928-021-00632-7>.
- Q. Shen, Y. Hao, L. Ma, X. Wang, Comparative Study of Red/Green/Blue Quantum-Dot Light-Emitting Diodes by Time-Resolved Transient Electroluminescence, *J. Phys. Chem. Lett.* 12 (2021) 7019–7025, <https://doi.org/10.1021/acs.jpcclett.1c01560>.
- E. Jang, S. Jun, H. Jang, J. Lim, B. Kim, Y. Kim, White-light-emitting diodes with quantum dot color converters for display backlights, *Adv. Mater.* 22 (2010) 3076–3080, <https://doi.org/10.1002/adma.201000525>.
- Y.H. Ko, P. Prabhakaran, S. Choi, G.J. Kim, C. Lee, K.S. Lee, Environmentally friendly quantum-dot color filters for ultra-high-definition liquid crystal displays, *Sci Rep* 10 (2020) 1–8, <https://doi.org/10.1038/s41598-020-72468-8>.
- A.Q. Xie, T. Cui, R. Cheng, X. Wu, J. Guo, X. Lu, L. Zhu, S. Chen, Robust Nanofiber Films Prepared by Electro-Microfluidic Spinning for Flexible Highly Stable Quantum-Dot Displays, *Adv. Electron. Mater.* 7 (2021) 2000626, <https://doi.org/10.1002/aelm.202000626>.
- H. Chen, J. He, S. Wu, Recent Advances on Quantum-Dot-Enhanced Liquid-Crystal Displays, *IEEE J Sel Top Quantum Electron* 23 (2017) 1–11, <https://doi.org/10.1109/JSTQE.2017.2649466>.
- M. Fröbel, F. Fries, T. Schwab, S. Lenk, K. Leo, M.C. Gather, S. Reineke, Three-terminal RGB full-color OLED pixels for ultrahigh density displays, *Sci. Rep.* 8 (2018) 9684, <https://doi.org/10.1038/s41598-018-27976-z>.
- Y. Huang, E.L. Hsiang, M.Y. Deng, S.T. Wu, Mini-LED, Micro-LED and OLED displays: present status and future perspectives, *Light Sci. Appl.* 9 (2020) 105, <https://doi.org/10.1038/s41377-020-0341-9>.
- H.J. Kim, M.H. Shin, H.G. Hong, B.S. Song, S.K. Kim, W.H. Koo, J.G. Yoon, S. Y. Yoon, Y.J. Kim, Enhancement of Optical Efficiency in White OLED Display Using the Patterned Photoresist Film Dispersed with Quantum Dot Nanocrystals, *J. Disp. Technol.* 12 (2016) 526–531, <https://doi.org/10.1109/JDT.2015.2503401>.
- M.C. Gather, A. Köhnen, K. Meerholz, White organic light-emitting diodes, *Adv. Mater.* 23 (2011) 233–248, <https://doi.org/10.1002/adma.201002636>.
- J.K. Lee, S. Cho, D.W. Kang, Analysis of light leakage between the adjacent pixels in a color-filter stacked white OLED display, *Displays* 45 (2016) 6–13, <https://doi.org/10.1016/j.displa.2016.09.001>.
- M. Duan, Z. Feng, Y. Wu, Y. Yin, Z. Hu, W. Peng, D. Li, S.-J. Chen, C.-Y. Lee, A. Lien, Inkjet-Printed Micrometer-Thick Patterned Perovskite Quantum Dot Films for Efficient Blue-to-Green Photoconversion, *Adv. Mater. Technol.* 4 (12) (2019) 1900779.
- Y. Li, Y. Wu, S. Zhang, W. Yuan, S. Zhang, S. Jiao, W. Peng, D. Li, P.-Y. Lu, 10.3: Invited Paper: A Novel QD-OLED Structure of High Optical Efficiency, *SID Symp. Dig. Tech. Pap.* 50 (2019) 100–102, <https://doi.org/10.1002/sdtp.13401>.
- Z. Hu, Y. Yin, M.U. Ali, W. Peng, S. Zhang, D. Li, T. Zou, Y. Li, S. Jiao, S.J. Chen, C. Y. Lee, H. Meng, H. Zhou, Inkjet printed uniform quantum dots as color conversion layers for full-color OLED displays, *Nanoscale*. 12 (2020) 2103–2110, <https://doi.org/10.1039/c9nr09086j>.
- L. Zhang, H. Liu, Y. Zhao, X. Sun, Y. Wen, Y. Guo, X. Gao, C.A. Di, G. Yu, Y. Liu, Inkjet printing high-resolution, large-area graphene patterns by coffee-ring lithography, *Adv. Mater.* 24 (2012) 436–440, <https://doi.org/10.1002/adma.201103620>.
- P. He, B. Derby, Controlling Coffee Ring Formation during Drying of Inkjet Printed 2D Inks, *Adv. Mater. Interfaces.* 4 (2017) 1700944, <https://doi.org/10.1002/admi.201700944>.
- Y. Liu, F. Li, L. Qiu, K. Yang, Q. Li, X. Zheng, H. Hu, T. Guo, C. Wu, T.W. Kim, Fluorescent microarrays of in situ crystallized perovskite nanocomposites fabricated for patterned applications by using inkjet printing, *ACS Nano* 13 (2019) 2042–2049, <https://doi.org/10.1021/acsnano.8b08582>.
- S. Shi, W. Bai, T. Xuan, T. Zhou, G. Dong, R.J. Xie, In Situ Inkjet Printing Patterned Lead Halide Perovskite Quantum Dot Color Conversion Films by Using Cheap and Eco-Friendly Aqueous Inks, *Small Methods*. 5 (2021) 2000889, <https://doi.org/10.1002/smtd.202000889>.
- Y. Wang, R. Deng, L. Yang, C.D. Bain, Fabrication of monolayers of uniform polymeric particles by inkjet printing of monodisperse emulsions prepared by microfluidics, *Lab Chip*. 19 (2019) 3077–3085, <https://doi.org/10.1039/c9lc00588a>.
- T. Tanaka, K. Kadota, Y. Tozuka, A. Shimosa, Y. Shirakawa, Improvement in photocatalytic activity of morphologically controlled Pd-supporting TiO₂ particles via sol-gel process using inkjet nozzle, *Ceram. Int.* 42 (2016) 9963–9971, <https://doi.org/10.1016/j.ceramint.2016.03.098>.
- S. Baek, S. Kim, J.Y. Noh, J.H. Heo, S.H. Im, K.H. Hong, S.W. Kim, Development of Mixed-Cation Cs₂Rb_{1-x}PbX₃ Perovskite Quantum Dots and Their Full-Color Film with High Stability and Wide Color Gamut, *Adv. Opt. Mater.* 6 (2018) 1800295, <https://doi.org/10.1002/adom.201800295>.
- Q. Zhou, Z. Bai, W.G. Lu, Y. Wang, B. Zou, H. Zhong, In Situ Fabrication of Halide Perovskite Nanocrystal-Embedded Polymer Composite Films with Enhanced Photoluminescence for Display Backlights, *Adv. Mater.* 28 (2016) 9163–9168, <https://doi.org/10.1002/adma.201602651>.
- Y. Wang, J. He, H. Chen, J. Chen, R. Zhu, P. Ma, A. Towers, Y. Lin, A.J. Gesquiere, S.T. Wu, Y. Dong, Ultrastable, Highly Luminescent Organic-Inorganic Perovskite-Polymer Composite Films, *Adv. Mater.* 28 (2016) 10710–10717, <https://doi.org/10.1002/adma.201603964>.
- X. Li, Y. Wu, S. Zhang, B. Cai, Y. Gu, J. Song, H. Zeng, CsPbX₃ Quantum Dots for Lighting and Displays: Room-temperature Synthesis, Photoluminescence Superiorities, Underlying Origins and White Light-Emitting Diodes, *Adv. Funct. Mater.* 26 (2016) 2435–2445, <https://doi.org/10.1002/adfm.201600109>.
- S.W. Dai, B.W. Hsu, C.Y. Chen, C.A. Lee, H.Y. Liu, H.F. Wang, H.C. Huang, T.L. Wu, A. Manikandan, R.M. Ho, C.S. Tsao, C.H. Cheng, Y.L. Chueh, Y.W. Lin, Perovskite Quantum Dots with Near Unity Solution and Near-Film Photoluminescent Quantum Yield by Novel Spray Synthesis, *Adv. Mater.* 30 (2018) 1705532, <https://doi.org/10.1002/adma.201705532>.
- D.W. Lee, M.C. Shin, Y.N. Kim, J.M. Oh, Brushite ceramic coatings for dental brace brackets fabricated via aerosol deposition, *Ceram. Int.* 43 (2017) 1044–1051, <https://doi.org/10.1016/j.ceramint.2016.10.037>.
- M.Y. Cho, S. Kim, I.S. Kim, E.S. Kim, Z.J. Wang, N.Y. Kim, S.W. Kim, J.M. Oh, Perovskite-Induced Ultrasensitive and Highly Stable Humidity Sensor Systems Prepared by Aerosol Deposition at Room Temperature, *Adv. Funct. Mater.* 30 (2020) 1907449, <https://doi.org/10.1002/adfm.201907449>.
- S. Kim, M.Y. Cho, I.S. Kim, W.J. Kim, S.H. Park, S. Baek, J.M. Oh, S.W. Kim, Solvent-Free Aerosol Deposition for Highly Luminescent and Thermally Stable Perovskite-Ceramic Nanocomposite Film, *Adv. Mater. Interfaces.* 6 (2019) 1900359, <https://doi.org/10.1002/admi.201900359>.
- M.Y. Cho, I.S. Kim, S.H. Kim, C. Park, N.Y. Kim, S.W. Kim, S. Kim, J.M. Oh, Unique Noncontact Monitoring of Human Respiration and Sweat Evaporation Using a CsPbBr₃-Based Sensor, *ACS Appl. Mater. Interfaces.* 13 (2021) 5602–5613, <https://doi.org/10.1021/acsaami.0c21097>.
- S. Baek, S. Kang, C. Son, S.J. Shin, J.H. Kim, J. Park, S.W. Kim, Highly Stable All-Inorganic Perovskite Quantum Dots Using a ZnX₂-Triocetylphosphine-Oxide: Application for High-Performance Full-Color Light-Emitting Diode, *Opt. Mater.* 8 (2020) 1901897, <https://doi.org/10.1002/adom.201901897>.
- J. Akedo, Room temperature impact consolidation (RTIC) of fine ceramic powder by aerosol deposition method and applications to microdevices, *J. Therm. Spray Technol.* 17 (2008) 181–198, <https://doi.org/10.1007/s11666-008-9163-7>.
- S. Kang, J.S. Huh, J.J. Kim, J. Park, Highly efficient deep-blue fluorescence OLEDs with excellent charge balance based on phenanthro[9,10-D] oxazole-anthracene derivatives, *J. Mater. Chem. C*. 8 (2020) 11168–11176, <https://doi.org/10.1039/d0tc01811b>.

- [40] S. Kang, H. Jung, H. Lee, S. Park, J. Kim, J. Park, Highly efficient dual-core derivatives with EQEs as high as 8.38% at high brightness for OLED blue emitters, *J. Mater. Chem. C* 7 (2019) 14709–14716, <https://doi.org/10.1039/c9tc04603h>.
- [41] T. Hatakeyama, A. Mizutani, T. Koike, ORGANIC ELECTROLUMINESCENT ELEMENT. United States patent US 16/092,856, 2019.
- [42] T. Hatakeyama, T. Koike, Y. Fujita, ORGANIC ELECTROLUMINESCENT ELEMENT. United States patent US 16/692,414, 2020.
- [43] V. Wood, M.J. Panzer, J. Chen, M.S. Bradley, J.E. Halpert, M.C. Bawendi, V. Bulović, Inkjet-printed quantum dot-polymer composites for full-color AC-driven displays, *Adv. Mater.* 21 (2009) 2151–2155, <https://doi.org/10.1002/adma.200803256>.
- [44] L. Shi, L. Meng, F. Jiang, Y. Ge, F. Li, X.-G. Wu, H. Zhong, In Situ Inkjet Printing Strategy for Fabricating Perovskite Quantum Dot Patterns, *Adv. Funct. Mater.* 29 (37) (2019) 1903648.
- [45] R. Xu, C. Qiao, M. Xia, B. Bai, Y. Li, J. Liu, J. Liu, H. Rong, M. Xu, J. Zhang, Stable quantum dots/polymer matrix and their versatile 3D printing frameworks, *J. Mater. Chem. C* 9 (2021) 7194–7199, <https://doi.org/10.1039/D1TC00861G>.
- [46] Q. Fu, W. Sun, Mie theory for light scattering by a spherical particle in an absorbing medium, *Appl. Opt.* 40 (2001) 1354–1361, <https://doi.org/10.1364/AO.40.001354>.
- [47] W. Hergert, T.h. Wriedt, *The Mie Theory: Basics and Applications*, Springer, Berlin, 2012.
- [48] C. Tan, Determination of refractive index of silica glass for infrared wavelengths by IR spectroscopy, *J Non Cryst Solids* 223 (1998) 158–163, [https://doi.org/10.1016/S0022-3093\(97\)00438-9](https://doi.org/10.1016/S0022-3093(97)00438-9).
- [49] M.J. Dodge, *Handbook of Laser Science & Technology, Optical Materials, Part 2 Vol. 4* (1986).
- [50] J. Song, K.H. Kim, E. Kim, C.K. Moon, Y.H. Kim, J.J. Kim, S. Yoo, Lensfree OLEDs with over 50% external quantum efficiency via external scattering and horizontally oriented emitters, *Nat. Commun.* 9 (2018) 3207, <https://doi.org/10.1038/s41467-018-05671-x>.
- [51] H.-Y. Lin, C.-W. Sher, D.-H. Hsieh, X.-Y. Chen, H.-M.-P. Chen, T.-M. Chen, K.-M. Lau, C.-H. Chen, C.-C. Lin, H.-C. Kuo, Optical cross-talk reduction in a quantum-dot-based full-color micro-light-emitting-diode display by a lithographic-fabricated photoresist mold, *Photonics Res.* 5 (2017) 411–416, <https://doi.org/10.1364/prj.5.000411>.
- [52] A. Mahajan, C.D. Frisbie, L.F. Francis, Optimization of aerosol jet printing for high-resolution, high-aspect ratio silver lines, *ACS Appl. Mater. Interfaces.* 5 (2013) 4856–4864, <https://doi.org/10.1021/am400606y>.
- [53] S. Zips, L. Grob, P. Rinklin, K. Terkan, N.Y. Adly, L.J.K. Weiß, D. Mayer, B. Wolfrum, Fully Printed μ -Needle Electrode Array from Conductive Polymer Ink for Bioelectronic Applications, *ACS Appl. Mater. Interfaces.* 11 (2019) 32778–32786, <https://doi.org/10.1021/acsami.9b11774>.
- [54] H. Zhang, B. Wang, B. Brown, Aerosol-Jet-Printed CoFe₂O₄Nanoparticle - Vertically Aligned Carbon Nanotube Composite for Microsupercapacitors, *J. Phys. Chem. C* 125 (2021) 7590–7597, <https://doi.org/10.1021/acs.jpcc.1c01154>.